



Article

Ionic Liquid Additives for Efficient and Durable Two-Step Perovskite Photovoltaic Devices

Fei Wang ^{1,2,†}, Yonggui Sun ^{2,†}, Taomiao Wang ^{2,†}, Guo Yang ², Qiannan Li ², Yongjun Li ², Haoran Lin ² ,
Xuejuan Wan ^{1,*}, Gang Li ^{3,*} and Hanlin Hu ^{2,*} 

¹ Shenzhen Key Laboratory of Polymer Science and Technology, College of Materials Science and Engineering, Shenzhen University, Shenzhen 518060, China; 321087@whut.edu.cn

² Hoffmann Institute of Advanced Materials, Postdoctoral Innovation Practice Base, Shenzhen Polytechnic, Nanshan District, Shenzhen 518055, China; 1221066811@njupt.edu.cn (Y.S.); 1221066812@njupt.edu.cn (T.W.); 22280078@mail.szpt.edu.cn (G.Y.); liqiannan@szpt.edu.cn (Q.L.); 1222067110@njupt.edu.cn (Y.L.); hlin@szpt.edu.cn (H.L.)

³ The Hong Kong Polytechnic University Shenzhen Research Institute, Shenzhen 518057, China

* Correspondence: wanxj@szu.edu.cn (X.W.); gang.w.li@polyu.edu.hk (G.L.); hanlinhu@szpt.edu.cn (H.H.)

† These authors contributed equally to this work.

Abstract: Ionic liquids (ILs) have found widespread use in controlling the crystallization process of perovskites, optimizing the morphology and enhancing the device performance, especially in the one-step method. However, research regarding the effects of ionic liquids on perovskite devices prepared using the two-step method remains relatively scarce. Here, an IL 1-Hexyl-3-methylimidazolium Tetrafluoroborate (HMIMBF₄) is selected as an additive in the perovskite precursor solution for the fabrication of PSCs using the two-step method. Our study involves a systematic exploration of the precise effects of ILs on the morphology of perovskite thin films, defect density, and photovoltaic performance. IL HMIMBF₄ is convincingly shown to possess a robust chemical affinity with perovskite components, thereby establishing a basis for the inhibition of ion migration. Concurrently, ILs play a pivotal role in governing the morphology of perovskite while also facilitating the conversion of lead iodide into the perovskite structure. Benefiting from the regulation of the perovskite morphology and defect states by IL HMIMBF₄, the devices with an efficiency exceeding 23% is ultimately achieved. Our research provides a comprehensive comprehension and contributes to advancing the utilization of ILs in two-step photovoltaic devices.

Keywords: ionic liquids; two-step method; photovoltaic devices; defect states



Citation: Wang, F.; Sun, Y.; Wang, T.; Yang, G.; Li, Q.; Li, Y.; Lin, H.; Wan, X.; Li, G.; Hu, H. Ionic Liquid Additives for Efficient and Durable Two-Step Perovskite Photovoltaic Devices. *Crystals* **2023**, *13*, 1370. <https://doi.org/10.3390/cryst13091370>

Academic Editor: Bo Chen

Received: 15 August 2023

Revised: 4 September 2023

Accepted: 6 September 2023

Published: 12 September 2023



Copyright: © 2023 by the authors. Licensee MDPI, Basel, Switzerland. This article is an open access article distributed under the terms and conditions of the Creative Commons Attribution (CC BY) license (<https://creativecommons.org/licenses/by/4.0/>).

1. Introduction

Hybrid organic–inorganic perovskite solar cells (PSCs), hailed as a promising form of printable solar technology, have garnered significant attention in research circles due to their impressive power conversion efficiencies (PCEs), outstanding light absorption capabilities, cost-effectiveness in manufacturing, and simple production processes, and the ability to tune their bandgap [1–6]. Over the last decade, the power conversion efficiencies (PCEs) of perovskite solar cells have shown remarkable progress, climbing from an initial debut of 3.8% to an impressive 26.1%, now comparable to those of commercial silicon solar cells [7,8]. Despite significant breakthroughs in the PCEs of PSCs, the persisting defects severely hinder the stability and further enhancement of the device’s efficiency [9].

In order to surmount the mentioned limiting factors, diverse additives have been incorporated into the perovskite precursor solution, aiming to regulate the crystal growth of perovskite and enhance the film morphology, which effectively mitigates the density of defects [10]. Ionic liquids (ILs) stand out among these additives as environmentally friendly and green options, primarily due to their nonvolatile nature. Furthermore, ILs provide various advantages such as the easy availability of the materials, high carrier mobility, solvating capabilities, as well as thermal and electrochemical stability [11,12]. These qualities

have found widespread application in perovskite solar cells, particularly in one-step fabrication methods. Wang and coworkers employed 1-butyl-3-methylimidazolium thiocyanate (BMIMSCN) ionic liquids as additives, effectively enhancing the quality of the perovskite film by forming a novel Pb-N bonding between the Pb^{2+} and ionic liquid [13]. With a significantly reduced defect density and improved carrier lifetime, their devices achieved an impressive champion PCE of 24.4% for small-area (0.148 cm^2) and 20.4% for larger-area (10.0 cm^2) configurations. Hu and colleagues incorporated 1,3-dimethylimidazolium iodide (DMII) ionic liquid into a perovskite precursor solution to passivate the vacancy defects of organic cations and halogen anions of perovskite in order to obtain high-quality perovskite film with enlarged grain sizes [14]. Although it has been confirmed that ILs play a significant role in the crystallization process and passivation of defects in perovskites, most of the current research is primarily focused on their application in one-step fabrication devices. Nonetheless, the majority of high-efficiency PSCs fabricated using the one-step method still rely on toxic anti-solvents, such as chlorobenzene (CB), dichloromethane (DCM), and toluene, which poses a hindrance to the commercialization of PSCs [15]. In comparison, the two-step method is widely recognized for providing enhanced repeatability and precise control over the crystallization process [16–19]. Unfortunately, there is relatively limited research on the use of ILs in the two-step fabrication process.

In this work, we incorporated IL 1-Hexyl-3-methylimidazolium Tetrafluoroborate (HMIMBF₄) as additives into the perovskite precursor solution to fabricate PSCs through the two-step method, and thoroughly investigated the specific impact of ILs on the morphology of perovskite thin films, defect density, and photovoltaic performance. Specifically, nuclear magnetic resonance spectroscopy (NMR), X-ray photoelectron spectroscopy (XPS) analysis, and Fourier-transform infrared spectroscopy (FTIR) were utilized to uncover the specific and strong interaction between the cation and anion in ILs with perovskite. The addition of ILs facilitated the transformation of lead iodide into perovskite, as confirmed by the results of the grazing-incidence wide-angle scattering measurements (GIWAXS) and XRD analyses. Furthermore, with the assistance of IL, there was a noticeable improvement in the morphology of the perovskite with larger grain sizes and reduced surface roughness, leading to a reduction in the number of grain boundaries and, consequently, a decrease in defects. Benefiting from the effective morphology regulation facilitated by ILs, this results in a mitigated charge-carrier recombination, prolonged photoluminescence (PL) lifetime, and significantly enhanced device performance. Consequently, the PSCs treated with ILs achieve a champion efficiency of 23.34%, outperforming the control device's efficiency of 21.45%. Our study offers an in-depth understanding and serves to promote the application of ILs in two-step photovoltaic devices.

2. Results and Discussion

In accordance with our previous studies, the perovskite thin film was fabricated using the conventional two-step sequential method [20]. For the preparation of IL-HMIMBF₄-treated perovskite film (Figure S1), IL HMIMBF₄ is incorporated into a PbI_2 solution in the first step and organic salts were subsequently applied over the PbI_2 layer, and then subjected to thermal annealing to create the modified perovskite film. The chemical structure of IL HMIMBF₄ is shown in Figure S2 and Fourier-transform infrared (FTIR) measurements are first conducted to analyze the interaction between IL HMIMBF₄ with PbI_2 (Figure 1a–c). For the corresponding spectra of IL HMIMBF₄ samples, the appearance of peaks at 1468 and 1170 cm^{-1} belong to the C=N and C-N vibrations which are attributed to the characteristic peaks of the imidazole group in IL HMIMBF₄. Upon the incorporation of PbI_2 in HMIMBF₄, the C=N and C-N peak values of HMIMBF₄ shift to 1463 and 1168 cm^{-1} , respectively. The shift of the peaks is explained by the strong chemical interaction of the imidazole group in the ILs with the PbI_2 . The corresponding shift in peak position has also been confirmed by other literature using ILs to form strong chemical interactions with PbI_2 . Meanwhile, the intensity of the corresponding characteristic peaks has not undergone obvious changes. To strengthen the credibility of our findings, we conducted a ¹H nuclear

magnetic resonance (NMR) spectra analysis on the HMIMBF₄ and HMIMBF₄-PbI₂ samples. The results, illustrated in Figure S3, demonstrate a noticeable chemical shift from 9.06 to 9.04 ppm in the resonance peaks of the imidazole group after adding PbI₂ to the HMIMBF₄ solution, which indicates the presence of co-ordination bonds between the C=N groups and unco-ordinated Pb²⁺. Moreover, the chemical shifts from 170.0 to 136.9 ppm in the ¹⁹F NMR spectra that belong to the BF₄⁻ signal in IL HMIMBF₄ further illustrate the connection between HMIMBF₄ and PbI₂ (Figure 1d). In pursuit of a deeper understanding, we conducted an X-ray photoelectron spectroscopy (XPS) analysis to examine the binding energies of the elements in both the control and HMIMBF₄-perovskite films, revealing the chemical interaction between HMIMBF₄ and the perovskite composition. As depicted in Figure 1e, two distinct peaks can be observed at 142.3 and 137.4 eV, corresponding to the Pb 4f_{5/2} and Pb 4f_{7/2} signals, respectively, in the control perovskite film. In contrast, the Pb 4f peaks in HMIMBF₄-modified films showed a noticeable shift toward lower binding energies (142.1 eV for 4f_{5/2} and 137.2 eV for 4f_{7/2}). This shift can be attributed to the electron donation from HMIMBF₄, which possesses a lone electron pair, to Pb²⁺⁺, leading to the formation of a Pb-N bond. Figure 1f displays the XPS spectra of I, indicating that, in the control perovskite films, two peaks are observed at 629.5 and 618.0 eV, corresponding to the binding energies of I 3d_{3/2} and I 3d_{5/2}, respectively. Following the HMIMBF₄ modification, the two peaks of I 3d exhibited a tendency to shift towards lower binding energies. These results indicate that ILs exhibit strong chemical interactions with the components of perovskite, providing a foundation for the crystallization regulation and inhibition of ion migration.

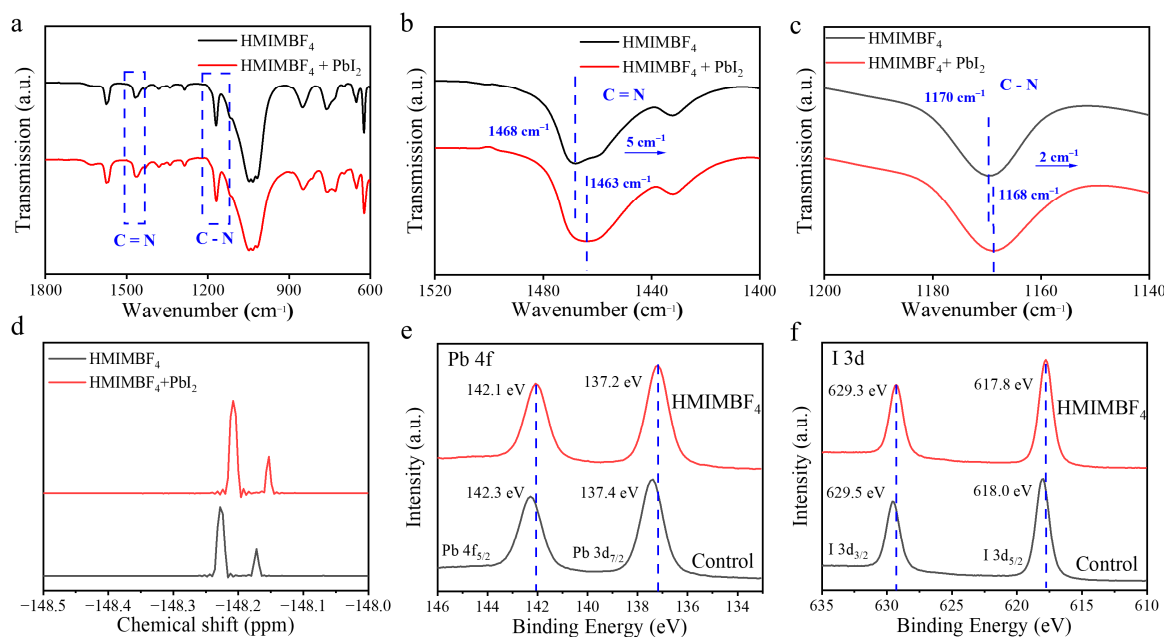


Figure 1. FTIR spectrum of IL HMIMBF₄ and HMIMBF₄-PbI₂ samples are presented in both general-view (a) and magnified forms (b,c). (d) ¹⁹F NMR spectrum of IL HMIMBF₄ and HMIMBF₄-PbI₂ samples. (e) Pb 4f and (f) I 1s XPS spectra of perovskite films.

The cross-sectional and top-view SEM are conducted to elucidate the impact of ILs on the structure of the PbI₂ film. Cross-sectional SEM images reveal that the original PbI₂ film exhibits a relatively dense layered structure, while the PbI₂ film modified with ILs displays a significant increase in pores within its layered structure in Figure 2a,b. Similarly, when examining the SEM images from a top-view perspective, a notable increase in the porosity of IL-modified PbI₂ becomes evident (Figure S4). It is important to note that the increased porosity of PbI₂ in the initial step of the two-step method facilitates the infiltration of organic salts in the subsequent step, thereby improving the residual presence of lead iodide

and promoting its transformation into perovskite. In order to demonstrate the presence of ILs in perovskite thin films, we performed EDS testing on perovskite thin films subjected to IL treatment. The EDS results indicate that the fluorine (F) and boron (B) elements present in the IL are uniformly and broadly distributed throughout the entire surface of the perovskite thin film, thus confirming the homogeneous distribution of the ionic liquid on the perovskite's surface (Figure S5). To investigate the impact of doping IL HMIMBF₄ on perovskite films, we obtained top-view SEM images of the control and HMIMBF₄-modified perovskite films for analysis, as illustrated in Figure 2c,d. In comparison to the pristine film, the HMIMBF₄-modified perovskite film displays enhanced uniformity in morphology and a distinct augmentation in grain size. Notably, the HMIMBF₄-modified perovskite thin film does not exhibit relatively small grain-sized perovskite crystals, as the presence of ILs significantly inhibits the formation of such small perovskite grains. In theory, the conventional solid-state grain growth mechanism has frequently been employed to elucidate the crystal growth of perovskite. The thermal annealing process induces Ostwald ripening and coarsening when a liquid phase is introduced into the perovskite grains. In our system, the nonvolatile IL HMIMBF₄ within the perovskite film provides a liquid microdomain, thus promoting grain growth through the Ostwald ripening coarsening mechanism. These findings are in strong agreement with previously reported observations in the literature [21]. The increase in grain size for the IL-assisted perovskite film is further confirmed by AFM, as depicted in Figure 2e,f. Additionally, the decreased surface roughness of the HMIMBF₄-modified perovskite film can be attributed to the larger grain size. Furthermore, the reduction in surface roughness observed in the HMIMBF₄-modified perovskite film can be ascribed to the control exerted over the perovskite's crystallization process through the introduction of IL. This control leads to the creation of smoother-surfaced crystals, consequently contributing to a decrease in surface roughness. The common salt KBF₄ was also employed to modulate the morphology of perovskite, and the corresponding SEM image is shown in Figure S6. From the results, it is shown that the grain size of KBF₄-treated perovskite is basically similar to that of the reference one, which is significantly smaller than that of the ionic liquid-modified film; therefore, ionic liquids possess a better modulation function compared with common salt to obtain a high-quality film.

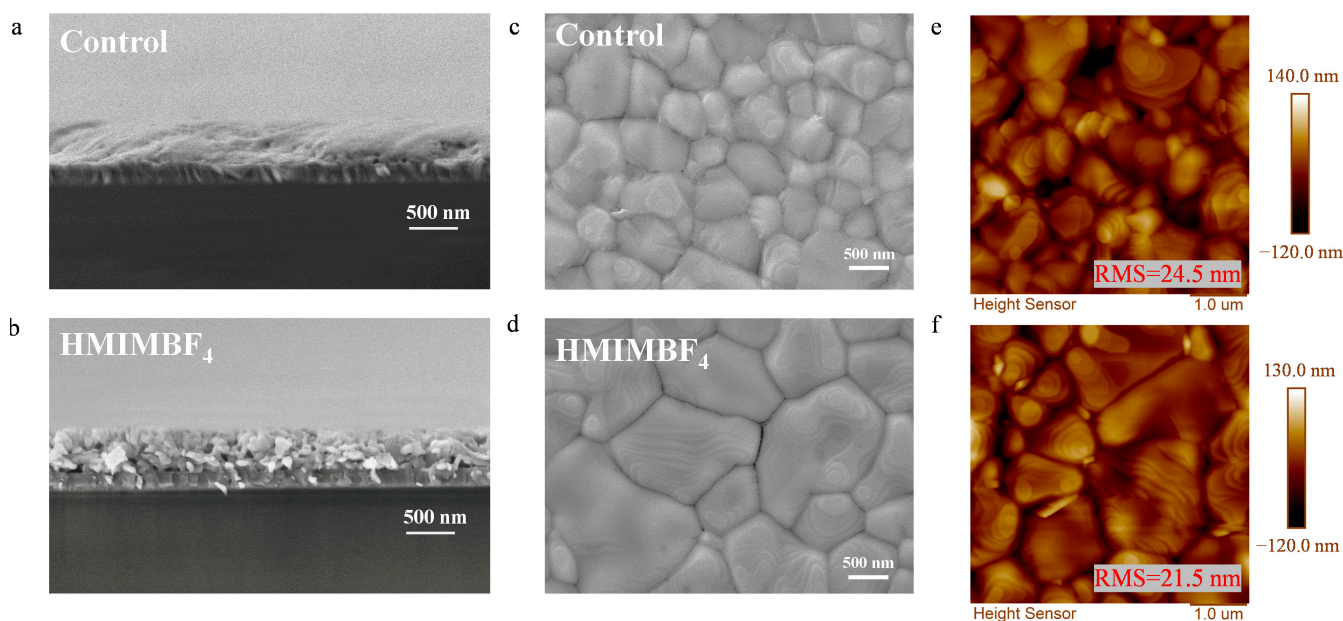


Figure 2. The cross-sectional SEM images of (a) control and (b) HMIMBF₄-modified PbI₂ film. SEM images of (c) control and (d) HMIMBF₄-modified perovskite films. (e,f) AFM images of perovskite films.

X-ray diffraction (XRD) patterns are acquired for both the unmodified and HMIMBF₄-modified perovskite films to gain a more comprehensive understanding of the impact of ILs on the perovskite films. An indistinguishable diffraction peak at 14.02°, corresponding to the (110) crystal plane of perovskite, is evident in both the unmodified and HMIMBF₄-modified perovskite films, as depicted in Figure 3a. This observation indicates that the incorporation of ILs has a negligible effect on polymorphism or lattice variation in the perovskite structure. In comparison to the control film, it is noteworthy that the intensity of the PbI₂ peak signal at 12.70° in the HMIMBF₄-modified films was significantly reduced, indicating the effective reduction of PbI₂ residue upon the addition of ILs. To further investigate the effect of IL HMIMBF₄ in promoting perovskite formation, systematic GIWAXS was conducted. Figure 3b,c present the 2D GIWAXS patterns of unmodified and HMIMBF₄-modified perovskite samples. Both samples exhibited two scattering peaks located at $q = 9$ and 10 nm^{-1} , which were attributed to the (110) planes of PbI₂ and the (110) planes of 3D perovskite crystals, respectively. Based on the 2D GIWAXS data, the radial integration outcomes for the samples are depicted in Figure 3d. In the unmodified perovskite film, a distinct peak at $q = 9 \text{ nm}^{-1}$ was observed, corresponding to the signal of PbI₂, which aligns with the traditional two-step references. In contrast, the signal of PbI₂ in the HMIMBF₄-modified perovskite samples was notably weaker, indicating that the addition of IL HMIMBF₄ facilitated the conversion of PbI₂ to perovskite. The presence of additives or solvents within the perovskite precursor solution can modify the morphology of the PbI₂ film via chemical interactions, effectively promoting the infiltration of organic salts and leading to a more complete transformation into perovskite. The excessive residual lead iodide in the two-step method is noteworthy as it can significantly contribute to the degradation of device stability. Effectively managing the residual lead iodide is of paramount importance in enhancing the photovoltaic performance and stability of the device [22]. Subsequently, UV-Vis (Figure 3e) and PL tests (Figure 3f) were conducted, revealing almost identical absorption thresholds and photoluminescence peak positions for both the unmodified and HMIMBF₄-modified perovskite films, indicating the retention of the lattice structure, which is consistent with the XRD findings. Furthermore, the results from the photoluminescence spectra reveal that, when compared to the control film, the HMIMBF₄-modified perovskite films exhibit stronger PL emission and a longer decay lifetime, as depicted in Figure 3f,g. These observations indicate the effective inhibition of the trap-mediated nonradiative recombination and the optimization of the perovskite film quality after the introduction of the IL HMIMBF₄. To further verify the impact of IL in the perovskite film on reducing non-radiative recombination centers under the same biasing voltage (Figure 3h,i), the electroluminescence intensity of the HMIMBF₄-treated device is notably stronger compared to the control devices, suggesting a significant reduction in the nonradiative recombination.

Subsequently, the trap state density (N_t) for the unmodified and HMIMBF₄-modified perovskite films in the devices with the structure of (ITO/SnO₂/perovskite/PCBM/Au) was numerically evaluated in Figure 4a,b. Notably, a smaller threshold voltage (V_{TFL}) of 0.197 V was observed in the HMIMBF₄-modified perovskite film compared to the control one with a V_{TFL} of 0.883 V. The value of N_t , calculated using the previously reported equation [23], was reduced from $1.4 \times 10^{16} \text{ cm}^{-3}$ to $3.2 \times 10^{15} \text{ cm}^{-3}$ in the HMIMBF₄-treated perovskite film (Figure 4c). These findings further support the conclusion that the addition of HMIMBF₄ leads to effective morphology control for obtaining high-quality film, resulting in a less nonradiative recombination and efficient carrier transport.

To gain comprehensive insights into the carrier transfer and recombination of the devices, electrochemical impedance spectroscopy (EIS) measurements were performed with a bias of 0 V (Figure 4d). The EIS curve exhibited two arcs in the high-frequency and low-frequency regions, corresponding to the charge transport resistance (R_{ct}) and the recombination resistance (R_{rec}), respectively. Compared to the control device, the HMIMBF₄-modified device showed a smaller R_{ct} and higher R_{rec} , suggesting an enhanced charge transport and diminished recombination. The carrier transport and recombination

in the devices were additionally assessed via conventional Mott–Schottky measurements employing capacitance–voltage analysis. The significant increase in the built-in potential (V_{bi}) from 0.84 V for the control device to 0.88 V for the HMIMBF₄-modified device is ascribed to the enhanced carrier transport and extraction (Figure 4e). Additionally, the HMIMBF₄-modified device displayed a reduced dark current density, indicating that the introduction of ILs improved the charge transport performance and decreased the leakage current (Figure 4f).

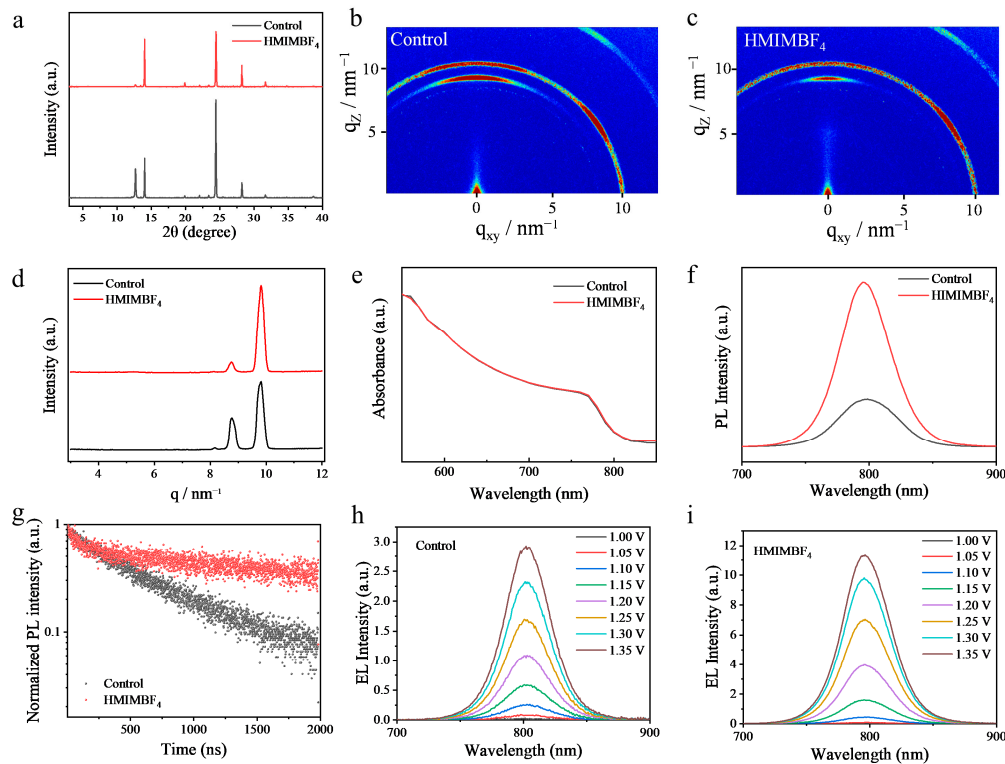


Figure 3. (a) X-ray diffraction spectra of unmodified and HMIMBF₄-modified perovskite films. The 2D GIWAXS patterns for (b) the unmodified and (c) HMIMBF₄-modified perovskite films. (d) Radial integration of 2D GIWAXS patterns for unmodified and HMIMBF₄-modified perovskite films. (e) UV-Visible absorption spectra of the unmodified and HMIMBF₄-modified perovskite films. (f) PL and (g) time-resolved PL spectra for the glass/unmodified and HMIMBF₄-modified perovskite samples. EQE-EL measurements for (h) control and (i) HMIMBF₄-modified PSCs under different biasing voltages.

For a more comprehensive exploration of the impact of IL modification on device performance, we fabricate PSC devices with and without an IL modification, utilizing a planar architecture of ITO/SnO₂/perovskite/Spiro-OMeTAD/Au (Figure 5a). Initially, cross-sectional scanning electron microscope (SEM) images are captured for both control and IL-treated complete devices, revealing evident variations in the morphology of the perovskite layers (depicted in Figure 5b,c). The IL-modified devices display significantly larger grains and a reduction in the number of grain boundaries, aligning well with the observations from top-view SEM images. To validate the enhancement of device performance by ILs, we optimized the concentration of the IL to find the optimal concentration for the ILs, and the photovoltaic parameters of devices treated with different concentrations of ILs are provided in the Figure S7. The photovoltaic parameters of devices treated with ILs at the optimum concentration exhibited significant improvements. Compared to a reference device with a PCE of 21.45%, the devices treated with ILs achieved a champion efficiency of 23.34% with the V_{oc} of 1.179, J_{sc} of 24.94, and FF of 79.37% (Figure 5d and Table S1). The significant improvement in efficiency after modification originates from

a marked enhancement in the quality of the perovskite thin film and a reduction in the defect density [24,25]. A substantial number of defects in the control perovskite thin films serve as non-radiative recombination centers, seriously affecting the carrier generation and transport. Inefficient carrier generation and transport, along with a higher amount of non-radiative recombination, will significantly impact the device's V_{oc} , leading to a decrease in the control devices' efficiency. The J_{SC} values obtained from the J - V curves of the PSCs treated with ILs closely align with the external quantum efficiency (EQE) results (24.00 mA cm^{-2}) obtained for the solar spectrum (Figure 5e). Furthermore, the efficiency distribution statistics for the devices are illustrated in Figure 5f. The control PSCs exhibit an average power conversion efficiency (PCE) of 20.13%, while the PSCs treated with HMIMBF₄ achieve an average PCE of 22.21%, exhibiting remarkable repeatability. The steady-state PCEs of the control and HMIMBF₄-treated PSCs were assessed using maximum power point tracking, demonstrating steady performance up to 20.89% and 23.00% (Figure S8), respectively. To further confirm the significant impact of the ionic liquid HMIMBF₄ on device performance, we systematically varied both the anion and cation of the ionic liquid. The corresponding photovoltaic parameters are provided in Tables S2 and S3. The results indicated that, regardless of changes in the anion or cation, HMIMBF₄ consistently exhibited the highest efficiency. This suggests that both the anion and cation of the ionic liquid play a significant role in enhancing the device performance. Furthermore, to demonstrate the advantages of using ionic liquids in the two-step method, we conducted a statistical analysis and comparison of the device performance's repeatability for both the one-step and two-step methods (Figure S9 and Table S4). The results showed that the repeatability and average efficiency of the two-step method were significantly higher than those of the one-step method.

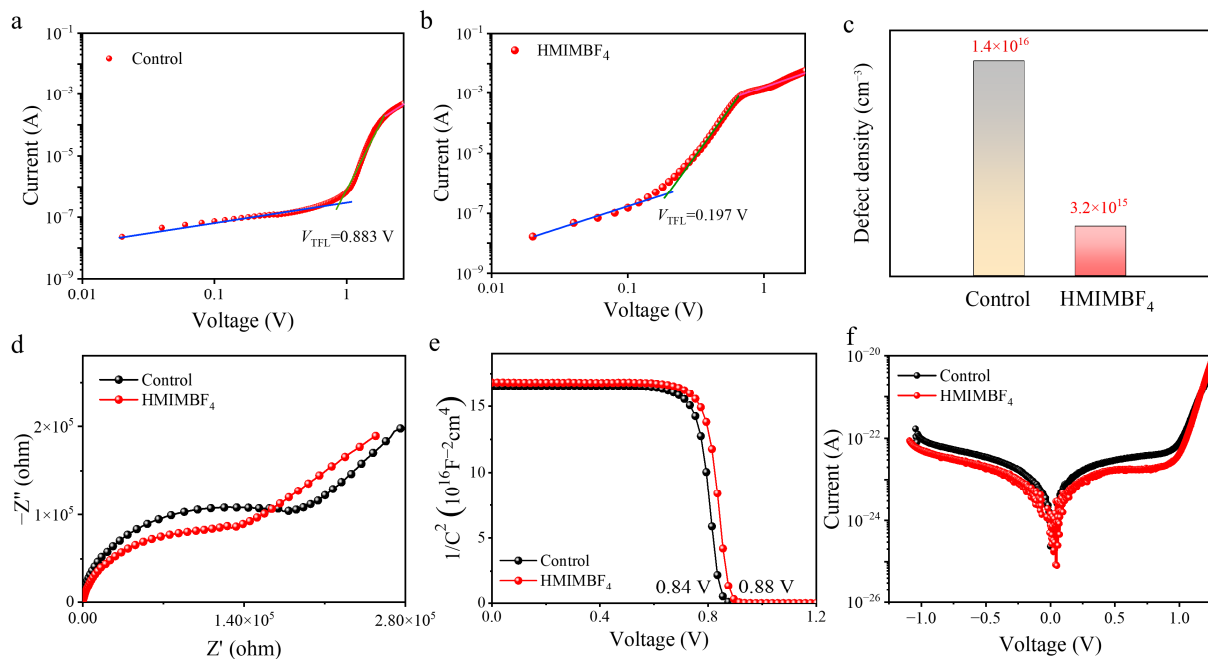


Figure 4. (a,b) Dark J - V curves of the devices with the structure of ITO/SnO₂/control or HMIMBF₄-treated perovskite/PCBM/Au. (c) Statistics for defect density computed from the dark J - V curves. (d) Nyquist plots and (e) J - V curves under dark conditions of unmodified and HMIMBF₄-modified devices. (f) Mott-Schottky plots of unmodified and HMIMBF₄-modified device.

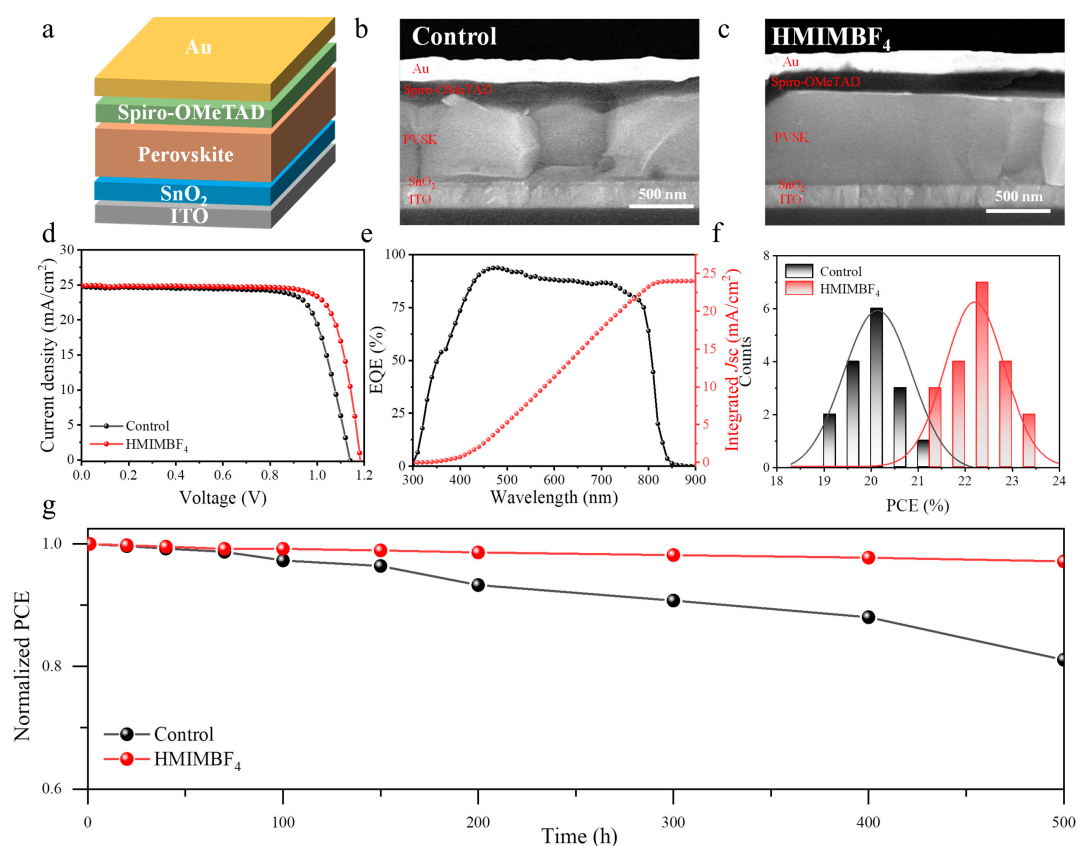


Figure 5. (a) The schematic diagram of the devices' structure. Cross-sectional SEM image of the (b) control and (c) HMIMBF₄-modified perovskite device structure. (d) *J*-*V* curves of the control and HMIMBF₄-modified PSCs. (e) EQE and the integrated *J*_{SC} of HMIMBF₄-PSCs. (f) Distribution statistics of control and HMIMBF₄-modified device efficiency. (g) Stability testing of devices.

Although the substantial enhancement in power conversion efficiency (PCE) is notable, ensuring the stability of photovoltaic solar cells (PSCs) remains a significant concern. ILs have emerged as promising candidates with which to replace conventional additives in the production of durable PSCs. The contact angle of the control and IL-treated perovskite film are obtained as shown in Figure S10, and the significant improvement from the reference value of 66° to 80°, indicating that the modification with ILs significantly enhances resistance to humidity. The stability assessment of the unencapsulated control and IL-treated perovskite PSCs is also conducted by tracking the PCE over time (Figure 5g). The unencapsulated IL-treated perovskite device shows an improved extended durability, maintaining 97.1% of its initial PCE even after 500 h in ambient dry air conditions. With the fluorinated poly(triarylamine) (1F-PTAA) as a hole-transport layer based on our previous study [26], the unencapsulated IL-treated perovskite device also exhibits decent thermal stability. It retains 88.9% of the initial PCE after 200 h at 80 °C in a glovebox. (Detailed information is available in Figures S11 and S12.)

3. Conclusions

In summary, we reported the utilization of an IL additive to optimize the photovoltaic performance of two-step method devices and systematically investigated the specific impact of ILs on the morphology of perovskite thin films, defect density, and photovoltaic performance. Notably, we employed various analytical techniques such as NMR, XPS analysis, and FTIR to unveil the pronounced interaction between ILs with perovskite. Moreover, ILs contributed to a significant improvement in perovskite morphology, characterized by larger grain sizes and reduced surface roughness. By harnessing the benefits of effective morphology optimization facilitated by ILs, charge-carrier recombination was

curbed, PL lifetime was prolonged, and device performance was remarkably enhanced. Consequently, PSCs treated with ILs achieved a champion efficiency of 23.34%, surpassing the 21.45% efficiency of the control device. Our comprehensive study not only deepens our understanding but also advances the application of ILs in two-step photovoltaic devices.

Supplementary Materials: The following supporting information can be downloaded at: <https://www.mdpi.com/article/10.3390/cryst13091370/s1>, Figure S1: Schematic diagram of Two-step preparation of perovskite films; Figure S2: Chemical structure of the IL HMIMBF₄; Figure S3: ¹H NMR spectra of HMIMBF₄ and HMIMBF₄+PbI₂ samples; Figure S4: The top-view SEM images of control and HMIMBF₄-modified PbI₂ film; Figure S5: EDS images of HMIMBF₄-modified perovskite film; Figure S6: SEM images of control, KBF₄ and HMIMBF₄-modified perovskite films; Figure S7: The statistics of photovoltaic performance parameters of HMIMBF₄-treated PSCs: PCE, Voc, FF and Jsc; Figure S8: Steady-state PCE of control and HMIMBF₄-treated PSCs by maximum power point tracking; Figure S9: The statistics of PCE of HMIMBF₄-treated PSCs via one-step and two-step, respectively. Figure S10: The water contact angle of the control and HMIMBF₄-perovskite film; Figure S11: Synthesize path for poly(triarylamine)(PTAA), fluorinated poly(triarylamine) (1F-PTAA and 2F-PTAA). (b) TGA curves of 1F-PTAA and (c) *J-V* curves for 1F-PTAA based ILs-assisted device. (d) Thermal stability results for both doped Spiro-OMeTAD and 1F-PTAA based ILs-assisted device at 80 °C in glove-box; Figure S12: (a–c) TGA curves of PTAA, 1F-PTAA and 2F-PTAA. and (d) *J-V* curve for 1F-PTAA based ILs-modified perovskite device. (d) Thermal stability results for 1F-PTAA based IL-modified perovskite device at 80 °C in glove-box; Table S1: Photovoltaic parameters of PSCs under AM 1.5G illumination at 100 mW cm⁻²; Table S2: Photovoltaic parameters of control, DMIMBF₄, BMIMBF₄ and HMIMBF₄-modified devices; Table S3: Photovoltaic parameters of control, HMIMI and HMIMBF₄-modified devices; Table S4: Photovoltaic parameters of HMIMBF₄-modified for one-step and two-step devices.

Author Contributions: Conceptualization, F.W. and H.H.; data curation, Y.S.; investigation, T.W., F.W., G.Y. and Y.S.; methodology, H.H., Q.L., Y.L. and F.W.; writing—original draft, X.W., G.L. and H.H.; writing—review and editing, H.H., X.W. and H.L.; visualization, H.H., X.W. and G.L.; supervision, H.H., X.W. and G.L.; project administration, H.H.; funding acquisition, H.H. All authors have read and agreed to the published version of the manuscript.

Funding: The financial support from Shenzhen Science and Technology Innovation Commission (Project No. JCYJ20200109105003940; Project No. 20220811205532001), Guangdong Basic and Applied Basic Research Foundation (No. 2023A1515011677)

Acknowledgments: The financial support from the Shenzhen Science and Technology Innovation Commission (Project No. JCYJ20200109105003940; Project No. 20220811205532001) and Guangdong Basic and Applied Basic Research Foundation (No. 2023A1515011677) is acknowledged.

Conflicts of Interest: The authors declare no conflict of interest

References

1. Jeon, N.J.; Noh, J.H.; Yang, W.S.; Kim, Y.C.; Ryu, S.; Seo, J.; Seok, S. II Compositional Engineering of Perovskite Materials for High-Performance Solar Cells. *Nature* **2015**, *517*, 476–480. [[CrossRef](#)]
2. Hui, W.; Chao, L.; Lu, H.; Xia, F.; Wei, Q.; Su, Z.; Niu, T.; Tao, L.; Du, B.; Li, D.; et al. Stabilizing Black-Phase Formamidinium Perovskite Formation at Room Temperature and High Humidity. *Science* **2021**, *371*, 1359–1364. [[CrossRef](#)]
3. Liang, C.; Gu, H.; Xia, Y.; Wang, Z.; Liu, X.; Xia, J.; Zuo, S.; Hu, Y.; Gao, X.; Hui, W.; et al. Two-Dimensional Ruddlesden–Popper Layered Perovskite Solar Cells Based on Phase-Pure Thin Films. *Nat. Energy* **2021**, *6*, 38–45. [[CrossRef](#)]
4. Wang, R.; Xue, J.; Wang, K.L.; Wang, Z.K.; Luo, Y.; Fenning, D.; Xu, G.; Nuryyeva, S.; Huang, T.; Zhao, Y.; et al. Constructive Molecular Configurations for Surface-Defect Passivation of Perovskite Photovoltaics. *Science* **2019**, *366*, 1509–1513. [[CrossRef](#)]
5. Zhu, J.; Luo, Y.; He, R.; Chen, C.; Wang, Y.; Luo, J.; Yi, Z.; Thiesbrummel, J.; Wang, C.; Lang, F.; et al. A Donor–Acceptor-Type Hole-Selective Contact Reducing Non-Radiative Recombination Losses in Both Subcells towards Efficient All-Perovskite Tandems. *Nat. Energy* **2023**, *8*, 714–724. [[CrossRef](#)]
6. Chen, Z.; Cheng, Q.; Chen, H.; Wu, Y.; Ding, J.; Wu, X.; Yang, H.; Liu, H.; Chen, W.; Tang, X.; et al. Perovskite Grain-Boundary Manipulation Using Room-Temperature Dynamic Self-Healing “Ligaments” for Developing Highly Stable Flexible Perovskite Solar Cells with 23.8% Efficiency. *Adv. Mater.* **2023**, *35*, 2300513. [[CrossRef](#)] [[PubMed](#)]
7. Zhao, Y.; Ma, F.; Qu, Z.; Yu, S.; Shen, T.; Deng, H.-X.; Chu, X.; Peng, X.; Yuan, Y.; Zhang, X.; et al. Inactive (PbI₂)₂RbCl Stabilizes Perovskite Films for Efficient Solar Cells. *Science* **2022**, *377*, 531–534. [[CrossRef](#)] [[PubMed](#)]
8. Min, H.; Lee, D.Y.; Kim, J.; Kim, G.; Lee, K.S.; Kim, J.; Paik, M.J.; Kim, Y.K.; Kim, K.S.; Kim, M.G.; et al. Perovskite Solar Cells with Atomically Coherent Interlayers on SnO₂ Electrodes. *Nature* **2021**, *598*, 444–450. [[CrossRef](#)] [[PubMed](#)]

9. Zhu, X.; Dong, H.; Chen, J.; Xu, J.; Li, Z.; Yuan, F.; Dai, J.; Jiao, B.; Hou, X.; Xi, J.; et al. Photoinduced Cross Linkable Polymerization of Flexible Perovskite Solar Cells and Modules by Incorporating Benzyl Acrylate. *Adv. Funct. Mater.* **2022**, *32*, 2202408. [[CrossRef](#)]
10. Liang, X.; Zhou, K.; Duan, D.; Wang, F.; Ge, C.; Zhou, X.; Yuan, M.; Shi, Y.; Lin, H.; Zhu, Q.; et al. Metal-Organic Framework Nanocrystals Enabled Efficient and Durable Two-Step Perovskite Photovoltaics. *Chem. Eng. J.* **2023**, *459*, 141524. [[CrossRef](#)]
11. Bai, S.; Da, P.; Li, C.; Wang, Z.; Yuan, Z.; Fu, F.; Kawecki, M.; Liu, X.; Sakai, N.; Wang, J.T.W.; et al. Planar Perovskite Solar Cells with Long-Term Stability Using Ionic Liquid Additives. *Nature* **2019**, *571*, 245–250. [[CrossRef](#)]
12. Wang, X.; Ran, X.; Liu, X.; Gu, H.; Zuo, S.; Hui, W.; Lu, H.; Sun, B.; Gao, X.; Zhang, J.; et al. Tailoring Component Interaction for Air-Processed Efficient and Stable All-Inorganic Perovskite Photovoltaic. *Angew. Chem. Int. Ed.* **2020**, *59*, 13354–13361. [[CrossRef](#)] [[PubMed](#)]
13. Wang, Y.; Yang, Y.; Li, N.; Hu, M.; Raga, S.R.; Jiang, Y.; Wang, C.; Zhang, X.; Lira-Cantu, M.; Huang, F.; et al. Ionic Liquid Stabilized Perovskite Solar Modules with Power Conversion Efficiency Exceeding 20%. *Adv. Funct. Mater.* **2022**, *32*, 2204396. [[CrossRef](#)]
14. Hu, P.; Huang, S.; Guo, M.; Li, Y.; Wei, M. Ionic Liquid-Assisted Crystallization and Defect Passivation for Efficient Perovskite Solar Cells with Enhanced Open-Circuit Voltage. *ChemSusChem* **2022**, *15*, e202200819. [[CrossRef](#)] [[PubMed](#)]
15. Han, Y.; Xie, H.; Lim, E.L.; Bi, D. Review of Two-Step Method for Lead Halide Perovskite Solar Cells. *Sol. RRL* **2022**, *6*, 2101007. [[CrossRef](#)]
16. Im, J.H.; Jang, I.H.; Pellet, N.; Grätzel, M.; Park, N.G. Growth of CH₃NH₃PbI₃ Cuboids with Controlled Size for High-Efficiency Perovskite Solar Cells. *Nat. Nanotechnol.* **2014**, *9*, 927–932. [[CrossRef](#)]
17. Jiang, Q.; Zhao, Y.; Zhang, X.; Yang, X.; Chen, Y.; Chu, Z.; Ye, Q.; Li, X.; Yin, Z.; You, J. Surface Passivation of Perovskite Film for Efficient Solar Cells. *Nat. Photonics* **2019**, *13*, 460–466. [[CrossRef](#)]
18. Zhou, T.; Xu, Z.; Wang, R.; Dong, X.; Fu, Q.; Liu, Y. Crystal Growth Regulation of 2D/3D Perovskite Films for Solar Cells with Both High Efficiency and Stability. *Adv. Mater.* **2022**, *34*, 2200705. [[CrossRef](#)]
19. Wu, Y.; Xu, G.; Xi, J.; Shen, Y.; Wu, X.; Tang, X.; Ding, J.; Yang, H.; Cheng, Q.; Chen, Z.; et al. In Situ Crosslinking-Assisted Perovskite Grain Growth for Mechanically Robust Flexible Perovskite Solar Cells with 23.4% Efficiency. *Joule* **2023**, *7*, 398–415. [[CrossRef](#)]
20. Wang, F.; Duan, D.; Zhou, K.; Xue, Y.Z.B.; Liang, X.; Zhou, X.; Ge, C.; Zhou, C.; Xiang, J.; Zhu, J.; et al. Ionic Liquid Engineering Enabled In-plane Orientated 1D Perovskite Nanorods for Efficient Mixed-dimensional Perovskite Photovoltaics. *InfoMat* **2023**, *5*, e12459. [[CrossRef](#)]
21. Lin, Z.; Su, Y.; Dai, R.; Liu, G.; Yang, J.; Sheng, W.; Zhong, Y.; Tan, L.; Chen, Y. Ionic Liquid-Induced Ostwald Ripening Effect for Efficient and Stable Tin-Based Perovskite Solar Cells. *ACS Appl. Mater. Interfaces* **2021**, *13*, 15420–15428. [[CrossRef](#)] [[PubMed](#)]
22. Zhang, Y.; Xu, L.; Wu, Y.; Zhang, H.; Zeng, F.; Xing, J.; Liu, B.; Qi, Y.; Dong, B.; Bai, X.; et al. Synergetic Excess PbI₂ and Reduced Pb Leakage Management Strategy for 24.28% Efficient, Stable and Eco-Friendly Perovskite Solar Cells. *Adv. Funct. Mater.* **2023**, *33*, 2214102. [[CrossRef](#)]
23. Wang, F.; Wai-Keung Fong, P.; Ren, Z.; Xia, H.-L.; Zhou, K.; Wang, K.; Zhu, J.; Huang, X.; Liu, X.-Y.; Wang, H.; et al. In-Depth Understanding of Ionic Liquid Assisted Perovskite Film Formation Mechanism for Two-Step Perovskite Photovoltaics. *J. Energy Chem.* **2022**, *73*, 599–606. [[CrossRef](#)]
24. Park, J.S.; Calbo, J.; Jung, Y.K.; Whalley, L.D.; Walsh, A. Accumulation of Deep Traps at Grain Boundaries in Halide Perovskites. *ACS Energy Lett.* **2019**, *4*, 1321–1327. [[CrossRef](#)]
25. Kaiser, W.; Hussain, K.; Singh, A.; Allothman, A.A.; Meggiolaro, D.; Gagliardi, A.; Mosconi, E.; De Angelis, F. Defect Formation and Healing at Grain Boundaries in Lead-Halide Perovskites. *J. Mater. Chem. A* **2022**, *10*, 24854–24865. [[CrossRef](#)]
26. Hu, H.; Qin, M.; Fong, P.W.K.; Ren, Z.; Wan, X.; Singh, M.; Su, C.J.; Jeng, U.S.; Li, L.; Zhu, J.; et al. Perovskite Quantum Wells Formation Mechanism for Stable Efficient Perovskite Photovoltaics—A Real-Time Phase-Transition Study. *Adv. Mater.* **2021**, *33*, 2006238. [[CrossRef](#)]

Disclaimer/Publisher's Note: The statements, opinions and data contained in all publications are solely those of the individual author(s) and contributor(s) and not of MDPI and/or the editor(s). MDPI and/or the editor(s) disclaim responsibility for any injury to people or property resulting from any ideas, methods, instructions or products referred to in the content.